Available online at www.sciencedirect.com

ScienceDirect

IFAC PapersOnline CONFERENCE PAPER ARCHIVE

IFAC PapersOnLine 52-12 (2019) 502–507

Application of LQG and $\mathcal{H}_\infty$ Gain Scheduling Techniques to Active Suppression of Flutter

Miguel Á Rosique * **Raheeg Alamin** * **James F Whidborne** *

* *Centre of Aeronautics, Cranfield University, Bedfordshire MK45 0AL, UK. email:raheeg.alamin;j.f.whidborne@cranfield.ac.uk*

Abstract: Aircraft flutter behaviour is highly dependent on flight conditions, such as airspeed, altitude and Mach number. Thus when closed-loop control is applied to suppress flutter, if these variations are taken into account then improved performance can be obtained if the controller has a certain degree of adaptivity to the variations. In this paper, a Linear Parameter-Varying (LPV) model of a rectangular wing including a trailing-edge control surface is considered. Two different gain scheduling controllers based on LQG and $\mathcal{H}_\infty$ techniques are designed to suppress flutter and reject perturbations. Simulations of the closed-loop system show that gain scheduling techniques are capable of fully stabilizing the system over the full range of the considered air velocity, and they increase flutter speed by more than 90%.

Keywords: Flexible structure control, Flutter, Aeroservoelasticity, LPV, Gain scheduling, $\mathcal{H}_\infty$, LQG.

1. INTRODUCTION

Of all the aeroelastic phenomena, flutter is one of the more important (Dowell, 2015, p. 53) as it leads to dynamic instability, and often leads to catastrophic structural failure (Dowell, 2015, p. 81). Essentially, it manifests itself when the airstream is supplying too much energy to the system, and then the system is not capable of dissipating it. In that case, the structure experiences divergent oscillations that might finally lead to catastrophic structural failure (García-Fogeda and Arévalo, 2014).

Historically, the flutter problem has been approached by means of passive methods. These methods rely on directly modifying the structure (introducing springs, additional masses, *etc.*) in order to change its stiffness and mass properties, so that flutter does not appear within the operating range of the aircraft (Karpel, 1981). More recently, active methods for flutter suppression have appeared as an alternative. These methods take advantage of closed-loop control engineering, and they are based on controllers that use the aircraft control surfaces at high frequencies to suppress flutter. This way, weight is not increased and the structural design can be enhanced in other aspects. However, these methods are not widespread in industry yet, but they will mean a tremendous advance in aircraft design in the coming years (Livine, 2018).

When designing active methods, we have to take into account that the flight conditions are rarely constant, but they change with time during a mission. Therefore, flutter suppression controllers that adapt to the changing conditions should have improved performance and stability margins compared to fixed gain linear controllers. Since the flight condition can be measured, gain scheduling controllers are suitable for flutter suppression since they adapt themselves to some measurable changing parameters of the system (Rugh and Shamma, 2000), allowing an increase in the flight envelope.

Gain scheduling, and in particular, LPV control has been widely proposed for regulating flutter. Possibly the first account is Blue and Balas (1997), who present an LFT model dependant on Mach number and dynamic pressure. The model is based on the NASA BACT model Scott et al. (2000). The study is extended in Barker and Balas (2000) to compare the LFT approach with a standard LPV approach. In Seiler et al. (2011), the approaches are extended to a model of the X-53 active aeroelastic wing. Another early account is Lau and Krener (1999) who develop a parameter-varying Ricatti equation approach based on the 3-DOF model of Küssner and Schwarz (1941). This model is the basis for several other studies, for example Prime et al. (2010), who, like Lau and Krener (1999) based their controller on LQR methods. Various other LPV modelling techniques have been used. For example, Al-Jiboory et al. (2017) use a variation of the gridding-based approach, whilst Baranyi (2006); Takarics and Baranyi (2013), use a tensor-product modelling technique.

In this paper, two different gain scheduling controllers are proposed to suppress flutter for an LPV model of a wing taken from Wright and Cooper (2007). The controllers are scheduled for varying-speed conditions between 50 and 200 m/s. The first controller uses splines to interpolate between a set of LQG compensators designed at different speeds. The weighting matrices for the LQR sub-problem are scheduled on the airspeed. The second controller uses the standard extension of $\mathcal{H}_\infty$ theory to affine and polytopic LPV systems (Apkarian et al., 1995), but a particular choice of LPV model polytope aids the procedure. The model schedules on the air velocity, but a subset of the

10.1016/j.ifacol.2019.11.293

overall parameter variation in the LPV model is geometrically constructed to reduce the conservatism.

In the next section, an overview of the dynamic wing modelling is provided. Sections 3 and 4 describe the LQG and $\mathcal{H}_\infty$ controller designs respectively. The disturbance rejection properties of the controllers are demonstrated by simulations, some results are presented in Section 5. Conclusions and further work are discussed in the final section.

2. DYNAMIC WING MODEL

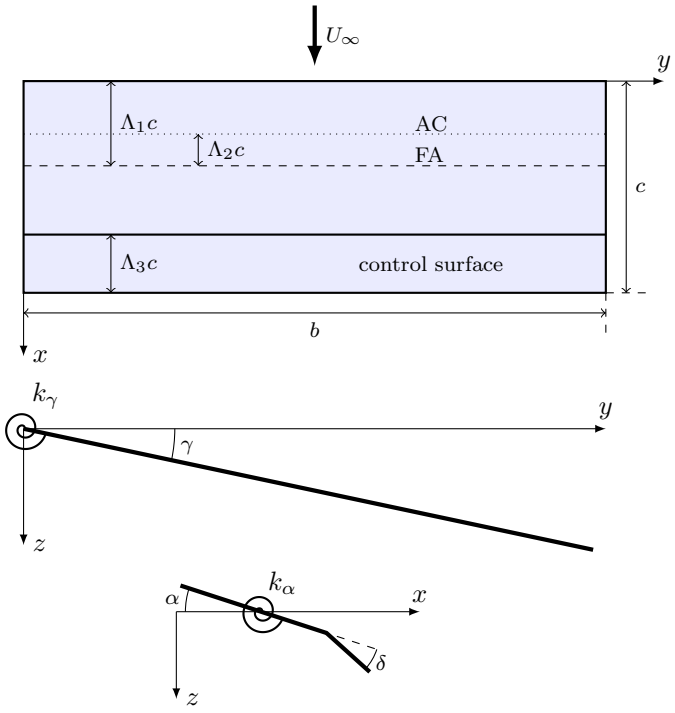

Fig. 1. Top, front and side view of the wing model.

A rectangular, untapered and unswept wing with no dihedral is considered in a flow with air velocity, U_∞. The wing presents a trailing edge control surface distributed along all the wing-span, b, which covers a fraction, Λ_3, of the wing chord, c. In the wing root, it is subjected to two rotational springs, one restraining the pitching angle α and the other one restraining the flapping angle γ. A sketch of the model is presented in Figure 1.

The flexural axis (FA) is assumed to be located at a distance $\Lambda_1 c$ of the leading edge, and the aerodynamic centre line (AC) is located a distance $\Lambda_2 c$ ahead of the flexural axis. The mass per unit surface of the wing is denoted by σ and it is assumed to be uniform for the entire wing and control surface. The deflection of the control surface is denoted by δ. The main characteristics of the model are summarized in Table 1. Note that the spring stiffness values are parameterized by the natural frequency of their isolated modes, which is related with the stiffness by:

$$k_i = I_i \omega_i^2, \quad i = \gamma, \alpha, \delta. \tag{1}$$

Small deformations and incompressible flow are considered, and air density at sea-level is assumed. For the aerodynamic forces we consider quasi-steady aerodynamics; it is considered that aerodynamic forces do not depend on past states of the system, and then they can be obtained using the steady problem formulation, but imposing the boundary condition corresponding to the unsteady body (Fung, 1969).

Table 1. Characteristics of the model.

b (m)	3.5	Λ_1	0.4	ω_γ (Hz)	5
c (m)	0.7	Λ_2	0.15	ω_α (Hz)	10
σ (kg/m^2)	100	Λ_3	0.275	ω_δ (Hz)	7.5

The basis of the model is taken from Wright and Cooper (2007), but an actuator model is included to model the phase lag between the demand in control surface deflection δ_d and the actual deflection

$$\tau_a \dot{\delta} = \delta_d - \delta. \tag{2}$$

After some manipulation of the equations, the system can be expressed as a first-order, descriptor, state-space system

$$\bar{\mathbf{E}}\dot{\mathbf{x}} = \bar{\mathbf{A}}(U_\infty)\mathbf{x} + \bar{\mathbf{B}}\delta_d \tag{3}$$

where the state variable vector is $\mathbf{x} = \begin{bmatrix}\gamma & \alpha & \dot{\gamma} & \dot{\alpha} & \dot{\delta}\end{bmatrix}^\intercal$, and

$$\bar{\mathbf{E}} = \begin{bmatrix} \mathbf{I}_{2\times 2} & \mathbf{0}_{2\times 2} & \mathbf{0}_{2\times 1} \\ \mathbf{0}_{2\times 2} & \widehat{\boldsymbol{\mathcal{M}}} & \mathbf{0}_{2\times 1} \\ \mathbf{0}_{1\times 2} & \mathbf{0}_{1\times 2} & \tau_a \end{bmatrix}, \tag{4}$$

$$\bar{\mathbf{A}} = \begin{bmatrix} \mathbf{0}_{2\times 2} & \mathbf{I}_{2\times 2} & \mathbf{0}_{2\times 1} \\ \frac{1}{\mu\tau_c^2}\widehat{\boldsymbol{\mathcal{Q}}}_1 - \omega_\alpha^2 \widehat{\boldsymbol{\mathcal{K}}} & \frac{1}{\mu\tau_c}\widehat{\boldsymbol{\mathcal{Q}}}_2 & \frac{1}{\mu\tau_c^2}\bar{\boldsymbol{\mathcal{Q}}}_1 \\ \mathbf{0}_{1\times 2} & \mathbf{0}_{1\times 2} & -1 \end{bmatrix}, \tag{5}$$

$$\bar{\mathbf{B}} = \begin{bmatrix} \mathbf{0}_{4\times 1} \\ 1 \end{bmatrix}, \tag{6}$$

and where the matrices $\widehat{\boldsymbol{\mathcal{M}}}$, $\widehat{\boldsymbol{\mathcal{K}}}$, $\widehat{\boldsymbol{\mathcal{Q}}}_1$, $\bar{\boldsymbol{\mathcal{Q}}}_1$ and $\widehat{\boldsymbol{\mathcal{Q}}}_2$ are non dimensional matrices that depend on the mass, stiffness and aerodynamic properties of the model; the parameter μ is the relation between the mass of the wing and the mass of an air cylinder of radius c and height b, $\mu = m_{wing}/(\pi c^2 b \rho_\infty)$; τ_c is the time the air takes to travel one chord, and ω_α is the natural frequency of the isolated pitching mode. Details of the mathematical development and expressions for the non-dimensional matrices are presented in Rosique (2018).

The descriptor state-space system (3) is rearranged to give a standard state-space model

$$\dot{\mathbf{x}} = \mathbf{A}(U_\infty)\mathbf{x} + \mathbf{B}\delta_d \tag{7}$$

where the state matrix $\mathbf{A}$ depends on the airspeed, so the model is an LPV system. Because the actuator acts as a filter, the input matrix $\mathbf{B}$ has no dependence on the air velocity.

It is assumed that the state of the system is not directly measured, but there is a sensor located at the mid-span and close to the hinge, measuring vertical displacement and its derivative (Andrés, 2017). This constitutes the output of the system $\mathbf{y}_m$ so that

$$\mathbf{y}_m = \begin{bmatrix} z \\ \dot{z} \end{bmatrix}_{\substack{x=(1-\Lambda_3)c \\ y=b/2}} \tag{8}$$

In order to design a controller, the relationship between the states and the output (matrix $\mathbf{C}$) has to be modelled.

Considering small deformations, the vertical displacement of the sensor and its derivative can be expressed as a function of the states:

$$\mathbf{y}_m = \begin{bmatrix} \mathbf{b_C^\intercal} & \mathbf{0}_{1\times 2} & 0 \\ \mathbf{0}_{1\times 2} & \mathbf{b_C^\intercal} & 0 \end{bmatrix} \mathbf{x} = \mathbf{C}\mathbf{x} \tag{9}$$

where $\mathbf{b_C^\intercal} = b/2\,[1 \;\; 2\Lambda\,(1-\Lambda_1-\Lambda_3)]$.

The open loop flutter speed of the model when the stiffness of the control surface hinge tends to infinity (for a rigid aerofoil) is calculated using the k-method (García-Fogeda and Arévalo, 2014). It turns out to be 99.55 m/s. This value decreases for a non-rigid hinge.

3. LQG CONTROLLER

The first controller is consists of state feedback with a Linear Qaudratic Regulator (LQR) and state estimation using a Linear Quadratic Estimator (LQE) in a standard Linear Quadratic Gaussian (LQG) compensator (Maciejowski, 1989, pp 222-227). The structure of the controller is shown in Figure 2.

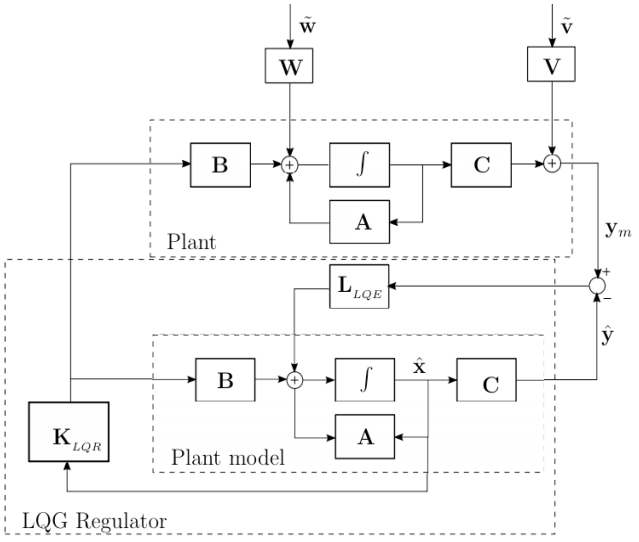

Fig. 2. Structure of the LQG compensator including an LQR for the control and an LQE to estimate the states from the output.

The LQR is an optimal controller that stabilizes the system and minimizes a cost function that is dependent upon the scheduled velocity condition. The cost function is designed to minimize the mechanical energy of the system, this is, to dissipate the energy supplied by the air to the system in order to avoid flutter. Taking into account that the mechanical energy of the system is given by the sum of the kinetic and potential energies:

$$\mathcal{E} = \frac{1}{2}\mathbf{q}^\intercal\mathbf{K}\mathbf{q} + \frac{1}{2}\dot{\mathbf{q}}^\intercal\mathbf{M}\dot{\mathbf{q}}, \tag{10}$$

and, after some manipulation, the cost function is expressed as a function of the normalized energy $\hat{\mathcal{E}} = \mathcal{E}/I_\gamma$ and a regularization term that takes into account the input of the system (control effort), so that

$$J = \int_0^\infty \left(\mathbf{x}^\intercal\mathbf{M_Q}\mathbf{x} + \mathbf{u}^\intercal\mathbf{M_R}\mathbf{u}\right) \mathrm{d}t \tag{11}$$

$$= \int_0^\infty \left(2\hat{\mathcal{E}} + \beta \left\|\mathbf{M_Q}\right\| {\delta_d}^2\right) \mathrm{d}t \tag{12}$$

where $\mathbf{M_R}$ is a scalar equal to $\beta\|\mathbf{M_Q}\|$, with $\beta = 0.05$ and the matrix $\mathbf{M_Q}$ is given by:

$$\mathbf{M_Q} = \begin{bmatrix} \omega_\alpha^2\widehat{\boldsymbol{\mathcal{K}}} & \mathbf{0}_{2\times 2} & \mathbf{0}_{2\times 1} \\ \mathbf{0}_{2\times 2} & \widehat{\boldsymbol{\mathcal{M}}} & \mathbf{0}_{2\times 1} \\ \mathbf{0}_{1\times 2} & \mathbf{0}_{1\times 2} & 0 \end{bmatrix} \tag{13}$$

and is dependent upon U_∞.

The controller that minimizes the cost function is different for each airspeed, so it has to be gain scheduled in order to adapt to the changes in the system. Although constant weighting matrices are used for the LQE, the gains of the LQE also change with airspeed, since these are dependent upon the state matrix, $A(U_\infty)$. Sixteen values of U_∞ between 50 m/s and 200 m/s are chosen, and LQG designs obtained. The LQR and LQE gains are interpolated using splines, in order to obtain a continuous gain scheduling LQG controller. Figure 3 shows how the gains of the LQR controller change with airspeed.

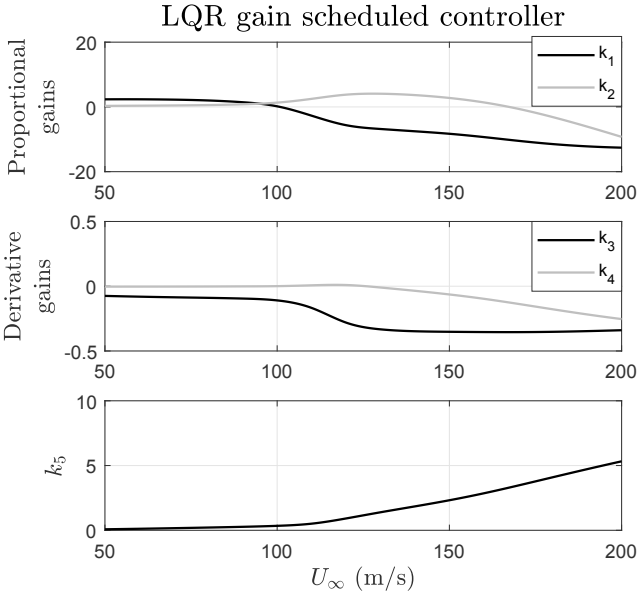

Fig. 3. Gains of the LQR controller as a function of velocity.

4. $\mathcal{H}_\infty$ CONTROLLER

The second gain scheduling controller is based on $\mathcal{H}_\infty$ techniques. $\mathcal{H}_\infty$-optimal control has been shown to be an effective and efficient robust design method for Linear, Time-Invariant (LTI) control systems (Gu et al., 2013); but the approach has been extended to time-varying systems by expressing the plant model as an affine combination of LTI systems multiplied by a set of time-varying coefficients (Apkarian et al., 1995), that is:

$$\mathbf{G} = \mathbf{G}_0 + \sum_{i=1}^{n} x_i\mathbf{G}_i. \tag{14}$$

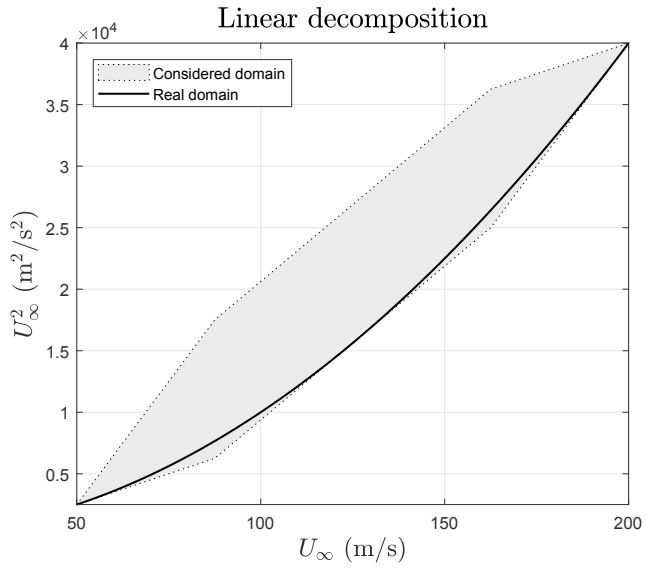

Fig. 4. Considered domain for the $\mathcal{H}_\infty$ controller when linearly decomposing the system.

The coefficients in the model given by (3) — (9) depend linearly on U_∞ and on U_∞^2, so (14) cannot be directly applied. One possible approach is to assume that the two parameters, $x_1 = U_\infty$ and $x_2 = U_\infty^2$, are independent of each other. However that would lead to an excessively conservative design since they are clearly not independent. A depiction of the relationship between x_1 and x_2 is shown in Figure 4. Assuming independence extends the parameter region from a parabola to a rectangle whose vertices are in the limit values for U_∞ and U_∞^2. In order to reduce the conservatism, we restrict U_∞ and U_∞^2 to a polytope that can also be expressed as an affine combination of a set of parameters expressed as the vector $\boldsymbol{\xi} = [\xi_1\ \xi_2\ \ldots]^\intercal$, so that

$$\begin{aligned} U_\infty &= a_0 + \sum_{i=1}^{n} a_i \xi_i, \\ U_\infty^2 &= b_0 + \sum_{i=1}^{n} b_i \xi_i, \end{aligned} \tag{15}$$

where $0 \leq \xi_i \leq 1$. By tuning the values of the coefficients a_i and b_i, we can reduce the considered domain and make it closer to the actual (real) one. We choose $n = 3$, as the domain is not significantly reduced for more parameters, and the controller is not very complicated. Introducing (15) in the model and after some manipulation, it can be expressed as the affine LPV model:

$$\mathbf{G} = \mathbf{G}_0 + \sum_{i=1}^{3} \xi_i \mathbf{G}_i. \tag{16}$$

Values of the coefficients a_i and b_i are summarized in Table 2, and the new domain is illustrated in Figure 4. The procedure for obtaining the values of the coefficients is explained in Rosique (2018). As we can see, the domain and the conservativeness is considerably reduced with respect to the first consideration. Note also that there remains some conservatism resulting from the symmetry of the envelope.

Given that the model is in the form of (14), we define the $\mathcal{H}_\infty$ condition to minimize the error $\mathbf{e}$ between the measured output and the null reference $\mathbf{w}$, and also the control signal $\mathbf{u}$. That leads to a standard *S over KS* problem (Gu et al., 2013) in which we search for a controller such that the following criterion is minimized:

$$\min_{\mathbf{K}} \left\| \begin{bmatrix} W_1\mathbf{S} \\ W_2\mathbf{KS} \end{bmatrix} \right\|_\infty, \tag{17}$$

where W_1 and W_2 are the loop-shaping weighting functions. Therefore, the controller aims to minimize the norm of the output signal $\mathbf{z}$. The structure of the closed loop configuration is shown in Figure 5.

Table 2. Values of the coefficients a_i and b_i for the linear decomposition of the system.

Coefficient	**0**	**1**	**2**	**3**
a_i (m/s)	50.0	37.5	75.0	37.5
b_i (m^2/s^2)	2500	3750	18750	15000

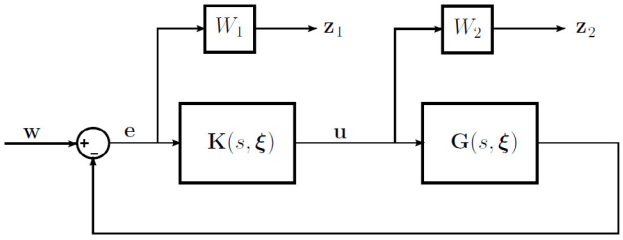

Fig. 5. Standard closed loop configuration and output signals $\mathbf{z}$.

The system has to be expressed in a standard $\mathcal{H}_\infty$ configuration, which is shown in Figure 6. Hence, we have to modify the original structure to obtain a plant $\mathbf{P}$ suitable for an $\mathcal{H}_\infty$-optimal controller.

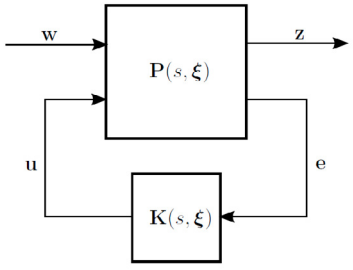

Fig. 6. Standard $\mathcal{H}_\infty$ configuration depending on the parameters ξ_i.

First, we consider an auxiliary plant $\mathbf{P}'$ that does not include the shaping filters W_i and whose state space representation can be expressed as:

$$\begin{aligned} \dot{\mathbf{x}} &= \mathbf{A}(\boldsymbol{\xi})\mathbf{x} + \mathbf{B}_1\mathbf{w} + \mathbf{B}_2\mathbf{u} \\ \mathbf{z}' &= \mathbf{C}_1\mathbf{x} + \mathbf{D}_{11}\mathbf{w} + \mathbf{D}_{12}\mathbf{u} \\ \mathbf{e} &= \mathbf{C}_2\mathbf{x} + \mathbf{D}_{21}\mathbf{w} + \mathbf{D}_{22}\mathbf{u} \end{aligned} \tag{18}$$

where the dependency on the velocity (or equivalently on the parameters ξ_i) appears only on the matrix $\mathbf{A}$, because that is the only matrix that depends on air velocity in (7). Taking into account (7), (9) and (18), and the structures presented in Figures 5 and 6, we obtain an expression for the different matrices characterizing the plant $\mathbf{P}'$ as

$$\mathbf{A} = \mathbf{A}(\boldsymbol{\xi}),$$
$$\mathbf{B}_1 = \mathbf{0}_{5\times 2}, \qquad \mathbf{B}_2 = \mathbf{B},$$
$$\mathbf{C}_1 = \begin{bmatrix} -\mathbf{C} \\ \mathbf{0}_{5\times 1} \end{bmatrix}, \qquad \mathbf{C}_2 = -\mathbf{C}$$
$$\mathbf{D}_{11} = \begin{bmatrix} \mathbf{I}_{2\times 2} \\ \mathbf{0}_{1\times 2} \end{bmatrix}, \qquad \mathbf{D}_{12} = \begin{bmatrix} \mathbf{0}_{2\times 1} \\ 1 \end{bmatrix},$$
$$\mathbf{D}_{21} = \mathbf{I}_{2\times 2}, \qquad \mathbf{D}_{22} = \mathbf{0}_{2\times 1}.$$

Once the plant $\mathbf{P}'$ is fully defined, $\mathbf{P}$ can be obtained by connecting $\mathbf{P}'$ in series with the loop-shaping functions W_1 and W_2 which are decided to be:

$$W_1 = \frac{2 \cdot 10^{-3}}{s + 10^{-3}}, \tag{19}$$

$$W_2 = \frac{0.02s}{s + 5000}, \tag{20}$$

where W_1 is designed as $W_1 = k/(s+\varepsilon)$ with $\varepsilon \to 0$, so that it is similar to an integrator (Su et al., 2000). When plant $\mathbf{P}$ is fully defined and properly expressed, the $\mathcal{H}_\infty$-optimal LPV controller is obtained using the `hinfgs` routine in MATLAB.

The variation in the controller gains is shown in Figure 7 by the singular value plots open-loop controllers at the eight vertices. The gains appear high, but the simulation results in the next section indicate that they are no excessive, and are of similar magnitude to the LQG controller.

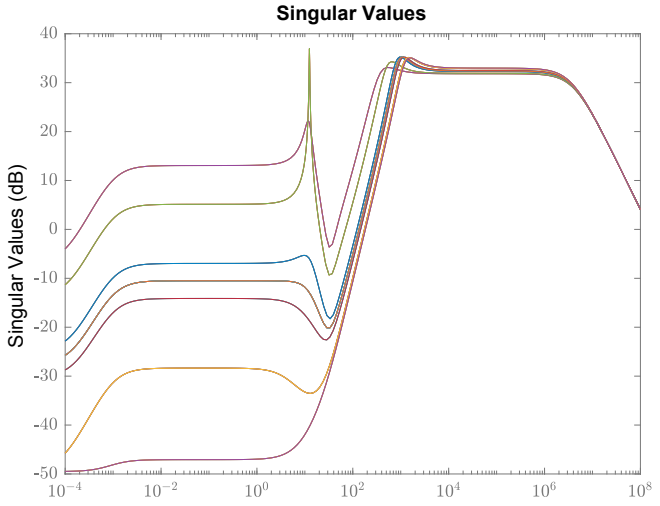

Fig. 7. $\mathcal{H}_\infty$ controller singular value plot for the 8 vertices.

5. SIMULATIONS AND RESULTS

Finally, some simulations are carried out to evaluate the performance of the considered approaches. Presented simulations test the disturbance rejection properties of the controllers. It is considered that the disturbances affect the control surface deflection. Therefore, they are injected into the system after the actuator dynamics; the structure is presented in Figure 8, in which the disturbance input is denoted by d. The transfer functions G_1 and G_2 correspond with the actuator model of (2) and the system of Figure 1 respectively. Equations for G_2 are not presented explicitly; they are similar to (3) but without including the actuator dynamics.

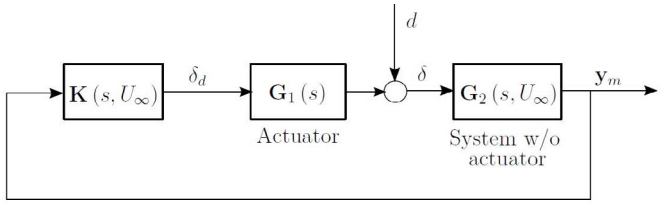

Fig. 8. Disturbances in the system scheme.

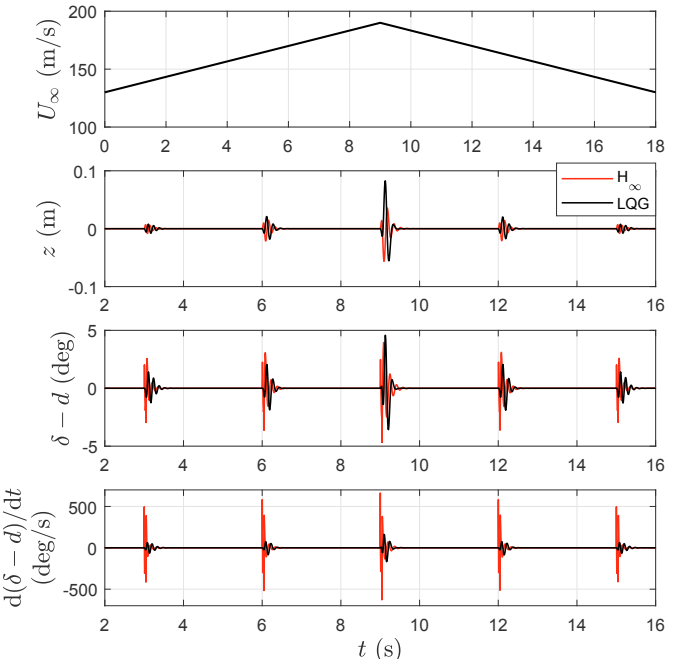

Fig. 9. Simulation for both LQG and $\mathcal{H}_\infty$ gain-scheduling controllers.

Short pulses of 1 degree amplitude and 0.04 seconds of duration are introduced as periodic disturbances in the system. The velocity is not constant during the simulations, but it varies linearly between 130 m/s and 190 m/s, first increasing and then decreasing, as it is shown in Figure 9. Both controllers are tested in the simulation. The results are presented in Figure 9, where three different variables are presented as output:

- Vertical displacement at the sensor location, which gives an estimation of the oscillations magnitude.
- Control surface deflection minus the value of the disturbances. This is the output of the actuator and it is an estimation of the control effort.
- Derivative of the previous magnitude. We also check the rates needed by the actuator, as they could condition performance.

Both gain scheduling controllers stabilize the system over the entire simulation, hence increasing the flutter speed to at least 190 m/s, an increase over the open loop value of more than 90%. Because the control is time varying, velocity has a relevant effect on the response; amplitude of the oscillations and control effort increase at higher speeds, making clear that is harder to suppress flutter at higher velocities.

The response of the $\mathcal{H}_\infty$ controller is more consistent with velocity; the responses to the different disturbances do not

present as much deviation among them as the LQG ones. Hence, this controller presents a higher adaptivity. Besides, the maximum value of z for this controller is 0.056 m (in absolute value), while it is 0.083 m for the LGQ regulator. Hence, $\mathcal{H}_\infty$ controller is more effective at suppressing the oscillations.

Regarding to the control signals, the maximum required control surface deflection is similar for both controllers (4.7 deg for $\mathcal{H}_\infty$ and 4.6 deg for LQG); but the required surface deflection rate is much higher for the $\mathcal{H}_\infty$ controller (660 deg/s) than for the LQG (162 deg/s). Although the $\mathcal{H}_\infty$ controller was more effective when suppressing oscillations, the LQG controller is more efficient; it obtains an acceptable performance but with much lower requirements in control rates. Of course, further tuning of the weighting functions can reduce the $\mathcal{H}_\infty$ controller deflection rates.

To summarize, both controllers present advantages and disadvantages, and it would be better to use one or another depending on the requirements and the available resources. Adaptivity of the controller is a key factor to ensure stability and properly suppress flutter; but the preferred control depends on each case.

6. CONCLUSIONS

The dynamic model of a generic rectangular wing has been developed for flutter study and active flutter suppression. The model is considered to be an LPV system dependent on airspeed, and the work focuses on the influence of velocity on flutter and how to handle airspeed variation. This is a general work that does not provide results for a single case, but it obtains general conclusions about flutter suppression. However, the model is considered to be linear for each certain value of the velocity (LPV), therefore, it is not valid for large displacements and it is limited to small disturbances.

Two different gain scheduling controllers based on LQG and $\mathcal{H}_\infty$ techniques were designed to suppress flutter. Both of them were able to increase the flutter speed by more than 90%, and they achieved stability and good system performance over the entire considered velocity range, due to their adaptivity. $\mathcal{H}_\infty$ controller was more effective when suppressing disturbance, whilst in this case the LQG regulator was more efficient as it required a lower control effort. Note that the MATLAB `systune` tool combined with tunable surfaces could be used to design gain scheduled controller in the structured $\mathcal{H}_\infty$ framework.

To conclude, it has been shown that active methods present a very high potential when it comes to flutter suppression, and they are capable of achieving very high increases in the flutter speed besides good performance in general. Adaptivity of the controllers is a key factor when the aircraft has to operate in changing conditions; therefore, gain scheduling control is a highly adequate technique to combine with closed-loop control for flutter suppression. Further simulations and robustness analysis remain for further investigation.

REFERENCES

Al-Jiboory, A.K., Zhu, G., Swei, S.S.M., Su, W., and Nguyen, N.T. (2017). LPV modeling of a flexible wing aircraft using modal alignment and adaptive gridding methods. *Aerospace Science and Technology*, 66, 92–102. doi:10.1016/j.ast.2017.03.009.

Andrés, E. (2017). *Active Suppression of Flutter by Feedback Control*. Master's thesis, Cranfield University.

Apkarian, P., Gahinet, P., and Becker, G. (1995). Self-scheduled $\mathcal{H}_\infty$ control of linear parameter-varying systems: a design example. *Automatica*, 31(9), 1251–1261. doi:10.1016/0005-1098(95)00038-X.

Baranyi, P. (2006). Tensor product model-based control of two-dimensional aeroelastic system. *Journal of Guidance, Control, and Dynamics*, 29(2), 391–400. doi:10.2514/1.9462.

Barker, J.M. and Balas, G.J. (2000). Comparing linear parameter-varying gain-scheduled control techniques for active flutter suppression. *Journal of Guidance, Control, and Dynamics*, 23(5), 948–955. doi:10.2514/2.4637.

Blue, P.A. and Balas, G. (1997). Linear parameter-varying control for active flutter suppression. In *Guidance, Navigation, and Control Conference*, AIAA-97-3640. New Orleans, LA. doi:10.2514/6.1997-3640.

Dowell, E.H. (2015). *A Modern Course in Aeroelasticity*. Springer, 5th edition.

Fung, Y.C. (1969). *An Introduction to the Theory of Aeroelasticity*. Dover Publications, New York.

García-Fogeda, P. and Arévalo, F. (2014). *Introducción a la Aeroelasticidad (Introduction to Aeroelasticity)*. Garceta, Madrid. In Spanish.

Gu, D., Petkov, P.H., and Konstantinov, M.M. (2013). *Robust Control Design with MATLAB*. Springer, 2nd edition.

Karpel, M. (1981). Design for active and passive flutter suppression and gust alleviation. Technical Report 3482, NASA.

Küssner, H.G. and Schwarz, I. (1941). The oscillating wing with aerodynamically balanced elevator. Technical Memorandum NACA TM 991, National Advisory Committee for Aeronautics.

Lau, E.Y. and Krener, A.J. (1999). LPV control of two dimensional wing flutter. In *Proceedings of the 38th IEEE Conference on Decision and Control*, 3005–3010. doi:10.1109/CDC.1999.831394.

Livine, E. (2018). Aircraft active flutter suppression: State of the art and technology maturation needs. *Journal of Aircraft*, 55(1), 410–452. doi:10.2514/1.C034442.

Maciejowski, J.M. (1989). *Multivariable Feedback Design*. Addison-Wesley, Wokingham, U.K.

Prime, Z., Cazzolato, B., Doolan, C., and Strganac, T. (2010). Linear-parameter-varying control of an improved three-degree-of-freedom aeroelastic model. *Journal of Guidance, Control, and Dynamics*, 33(2), 615–619. doi:10.2514/1.45657.

Rosique, M.A. (2018). *Active Flutter Suppression by Gain Scheduling Control*. Master's thesis, Cranfield University.

Rugh, W.J. and Shamma, J.S. (2000). Research on gain scheduling. *Automatica*, 36(10), 1401–1425. doi:10.1016/S0005-1098(00)00058-3.

Scott, R.C., Hoadlet, S.T., Wieseman, C.D., and Durham, M.H. (2000). Benchmark active controls technology model aerodynamic data. *Journal of Guidance, Control, and Dynamics*, 23(5), 914–921. doi:10.2514/2.4632.

Seiler, P., Balas, G., and Packard, A. (2011). Linear parameter varying control for the X-53 active aeroelastic wing. In *AIAA Atmospheric Flight Mechanics Conference, Guidance, Navigation, and Control and Co-located Conferences*, AIAA 2011-6290. Portland, OR. doi:10.2514/6.2011-6290.

Su, S.W., Anderson, B.D.O., and Brinsmead, T.S. (2000). Robust disturbance suppression for nonlinear systems based on $\mathcal{H}_\infty$ control. *Proceedings of the 39th Conference on Decision and Control*, 3013–3018. doi:10.1109/CDC.2000.914281.

Takarics, B. and Baranyi, P. (2013). Tensor-product-model-based control of a three degrees-of-freedom aeroelastic model. *Journal of Guidance, Control, and Dynamics*, 36(5), 1527–1533. doi:10.2514/1.57776.

Wright, J.R. and Cooper, J.E. (2007). *Introduction to Aircraft Aeroelasticity and Loads*. Wiley, Chichester.

2019-11-23

þÿ A p p l i c a t i o n o f L Q G a n d H" g a i scheduling techniques to active suppression of flutter

Rosique, Miguel Á.

Elsevier

þÿ R o s i q u e M A , A l a m i n R , W h i d b o r n e J F . (2 0 1 9) A p p l i c a t i o n o f L Q G a n d H" techniques to active suppression of flutter. IFAC-PapersOnLine, Volume 52, Issue 12, 2019, pp. 502-507 https://doi.org/10.1016/j.ifacol.2019.11.293